Experimental Animals
Exp. Anim. 71(3), 316–328, 2022

Original

Organoid technology and lung injury mouse models evaluating effects of hydroxychloroquine on lung epithelial regeneration

Fuxiaonan ZHAO[1)]*, Jianhai WANG[1,2)]*, Qi WANG[3)]*, Zhili HOU[1,3)]*, Yingchao ZHANG[4)]*, Xue LI[1,2,5)], Qi WU[1)] and Huaiyong CHEN[1,2,3,5)]

[1)]*Department of Basic Medicine, Haihe Clinical School, Tianjin Medical University, No. 890 Jingu Road, Shuanggang Town, Jinnan District, Tianjin 300350, P.R. China*
[2)]*Department of Basic Medicine, Haihe Hospital, Tianjin University, No. 890 Jingu Road, Shuanggang Town, Jinnan District, Tianjin 300350, P.R. China*
[3)]*Key Research Laboratory for Infectious Disease Prevention for State Administration of Traditional Chinese Medicine, Tianjin Institute of Respiratory Diseases, No. 890 Jingu Road, Shuanggang Town, Jinnan District, Tianjin 300350, P.R. China*
[4)]*Department of Pulmonary and Critical Care Medicine, Tianjin Baodi Hospital, Baodi Clinical College of Tianjin Medical University, No. 8 Guangchuan Road, Baodi District, Tianjin 300350, P.R. China*
[5)]*Tianjin Key Laboratory of Lung Regenerative Medicine, No. 890, Jingu Road, Shuanggang Town, Jinnan District, Tianjin 300350, P.R. China*

Abstract: Severe acute respiratory syndrome coronavirus 2 (SARS-CoV-2) damages lung epithelial stem/progenitor cells. Ideal anti-SARS-CoV-2 drug candidates should be screened to prevent secondary injury to the lungs. Here, we propose that *in vitro* three-dimensional organoid and lung injury repair mouse models are powerful models for the screening antiviral drugs. Lung epithelial progenitor cells, including airway club cells and alveolar type 2 (AT2) cells, were co-cultured with supportive fibroblast cells in transwell inserts. The organoid model was used to evaluate the possible effects of hydroxychloroquine, which is administered as a symptomatic therapy to the coronavirus disease 2019 (COVID-19) patients, on the function of mouse lung stem/progenitor cells. Hydroxychloroquine was observed to promote the self-renewal of club cells and differentiation of ciliated and goblet cells *in vitro*. Additionally, it inhibited the self-renewal ability of AT2 cells *in vitro*. Naphthalene- or bleomycin-induced lung injury repair mouse models were used to investigate the *in vivo* effects of hydroxychloroquine on the regeneration of club and AT2 cells, respectively. The naphthalene model indicated that the proliferative ability and differentiation potential of club cells were unaffected in the presence of hydroxychloroquine. The bleomycin model suggested that hydroxychloroquine had a limited effect on the proliferation and differentiation abilities of AT2 cells. These findings suggest that hydroxychloroquine has limited effects on the regenerative ability of epithelial stem/progenitor cells. Thus, stem/progenitor cell-derived organoid technology and lung epithelial injury repair mouse models provide a powerful platform for drug screening, which could possibly help end the pandemic.
Key words: alveolar type 2 (AT2) cells, club cells, epithelial regeneration, lung organoids, mouse model

Introduction

The coronavirus disease 2019 (COVID-19) broke out in December 2019, which has affected the population of more than 200 countries and regions globally. Currently, the number of confirmed cases of COVID-19 worldwide exceeds 220 million and the death toll has reached 4.5 million. COVID-19 is clinically divided into the follow-

(Received 24 September 2021 / Accepted 20 January 2022 / Published online in J-STAGE 22 February 2022)
Corresponding authors: H. Chen. email: huaiyong.chen@foxmail.com
Q.WU. email: wq572004@163.com
**These authors contributed equally to this work.*
Supplementary Figures: refer to J-STAGE: https://www.jstage.jst.go.jp/browse/expanim

ing levels based on its severity: mild to moderate, severe, and critical (respiratory failure) [1]. Common symptoms include fever, cough, and muscle pain [2], and patients with this disease often display the following lung histopathological features: lung epithelial injury, hyaline membrane formation, and diffuse inflammatory infiltration [3, 4].

Epithelial stem/progenitor cells, including club and type 2 alveolar (AT2) cells, reside in the intralobar conducting airways and alveoli of the human lung, respectively. When the lung epithelium is injured, these cells can self-renew to regenerate and repair the lung epithelium. Once the repair is completed, the structure and function of the lung are restored [5, 6]. Club cells generate ciliated and goblet cells through proliferation and differentiation, whereas AT2 cells can differentiate into AT1 cells, which are necessary for gas exchange [7–9]. Severe acute respiratory syndrome coronavirus 2 (SARS-CoV-2) invades cells through its spike protein to bind to the angiotensin-converting enzyme 2 (ACE2) receptor [10]. Because ACE2 receptors are expressed on the surface of club cells and AT2 cells, these two epithelial progenitor cells can be targeted and damaged by SARS-CoV-2 [11]. A diminished pool of lung progenitor cells may compromise the regenerative capacity of the epithelium and slow down the restoration of epithelial barrier. Consistent with this, SARS-CoV-2 infection-induced lung damage in COVID-19 patients has been proposed to persist for a long time [12]. Xu *et al.* confirmed an increase in the mRNA expression of transforming growth factor β, connective tissue growth factor, and fibronectin (Fn1) in the lung epithelial cells of patients with COVID-19 [13]. This increase was found to result in Fn1 deposition, which is indicative of potential pulmonary fibrosis in patients with COVID-19. Therefore, clinical medicine prescribed for COVID-19 patients should be screened to avoid secondary injury to the lung epithelial progenitor cells to reduce the occurrence of lung fibrotic progression.

A stem/progenitor cell-derived 3-D organoid culture technology shows great potential for evaluating drug safety and investigating host-pathogen interactions. Using this organoid model, Lamers *et al.* demonstrated that a low dose of interferon λ1 can reduce SARS-CoV-2 replication [14]. Mulay *et al.* used this model to study the efficacy of COVID-19 drug candidates and confirmed that remdesivir strongly inhibits SARS-CoV-2 infection/replication [15]. As the distribution and function of club and AT2 cells in the lungs of mice is very similar to that of humans, mouse models can be used to examine the changes in club and AT2 cells [16]. Naphthalene (Naph) is an environmental toxicant that can cause cancer [17]. Naph-induced airway epithelial injury and repair models have been widely recognized and applied [17, 18]; Hsu *et al.* used this model to demonstrate the important role of β-catenin in the proliferation and self-renewal of airway epithelial cells [19]. Bleomycin (BLM), an antitumor drug, has been shown to induce AT2 cell apoptosis and lung fibrosis [20]. We previously adopted this mouse model to demonstrate that the weight-reducing drug orlistat appeared to counteract the effects of autophagy loss on alveolar epithelial injury [21]. Both *in vitro* organoid culture and *in vivo* lung injury mouse models provide opportunities to evaluate drug safety in regenerative medicine.

To date, there are no effective drugs to treat COVID-19 patients. Several potential anti-SARS-CoV-2 drug candidates have been proposed and clinically tested. For example, remdesivir can block the viral life cycle by inhibiting the viral RNA-dependent RNA polymerase [22]. However, its efficacy in treating COVID-19 remains controversial [23, 24]. Hydroxychloroquine (HCQ) can inhibit glycosylation of the host receptor and increase the pH of the endosome to prevent viruses from entering cells. It exerts antiviral effects by regulating activated immune cells [25]. Some studies have suggested that HCQ treatment has a beneficial effect on COVID-19 patients, such as increased pneumonia improvement rate, faster fever reduction, and lower mortality [26, 27]. However, other studies have shown that HCQ is not helpful in treating COVID-19 patients [28–30]. Besides, there are various adverse reactions associated with the use of HCQ [31, 32]. The use of HCQ may be associated with an increased risk of arrhythmia [32–34]. Several research teams have shown that HCQ may increase tissue damage, including that of the lung [35–37]. In the present study, we used *in vitro* organoid cultures and mouse lung epithelial injury models to evaluate the effect of HCQ on the regeneration of club and AT2 cells. Our findings suggest that HCQ has limited effects on the regenerative ability of the lungs.

Materials and Methods

Compounds

Hydroxychloroquine sulfate (HCQ) was purchased from Shanghai Macklin Biochemical Co., Ltd. (Shanghai, China) and solubilized in sterile water as recommended. And the compounds used are from the same batch.

Animals

Male C57BL/6J mice (age, 6–10 week-old) were purchased from Beijing Huafukang Bioscience, China, and housed in a fixed location in a specific pathogen-free (SPF) facility at Tianjin University Haihe Hospital.

Animals were randomly assigned to control and treatment groups. Their age and gender were matched. For each animal, different investigators are responsible for the damage, treatment, harvest and result processing. The mouse study was approved by the Haihe Hospital Animal Care and Use Committee (approval number: 2020HHSQKT-047).

Naphthalene-induced mouse airway epithelial injury

Before 10 am, 250 mg/kg naphthalene (Sigma, St. Louis, MO, USA) dissolved in corn oil (Sigma) was intraperitoneally injected into the mice. HCQ or phosphate-buffered saline (PBS) (Gibco, Grand Island, NY, USA) was administered at a fixed time for 7 and 14 days, after naphthalene. The Ethics Committee of Haihe Hospital, Tianjin University provided approval (ethical approval number: 2020HHSQKT-047).

Bleomycin (BLM)-induced mouse alveolar epithelial injury

Mice were anesthetized using 7.5% chloral hydrate (Sangon Biotech, Shanghai, China), followed by a single intratracheal administration of BLM (2 U/kg body weight, Nippon Kayaku, Tokyo, Japan). Mice received HCQ (10 mg/kg or 50 mg/kg, i.p.) or PBS on day 1 after BLM, as previously described [21]. Thereafter, HCQ or 1 × PBS was administered at a fixed time for 7 and 14 days. Mice were sacrificed on days 7 and 14 after the HCQ administration. The Ethics Committee of Haihe Hospital, Tianjin University provided approval (ethical approval number: 2020HHSQKT-047).

Fluorescence-activated cell sorting (FACS)

A single-cell suspension was prepared by digestion of lung tissues from 6–10-week-old C57BL/6 mice with elastase and DNase I. Freshly isolated cells were suspended in Hanks balanced saline solution (Solarbio, Beijing, China) with 2% fetal bovine serum (FBS, Gibco), 0.01% Penicillin- streptomycin (Gibco, USA) and 10 mM HEPES (Sigma). The primary antibodies used to stain cells included CD24-PE (1:25, eBioscience, San Diego, CA, USA), EpCAM-PE-Cy7 (1:50, Biolegend, San Diego, CA, USA), CD31-biotin (1:50, eBioscience), CD45-biotin (1:100, eBioscience), CD34-biotin (1:16, eBioscience), and Sca-1-APC (1:100, eBioscience). Then, the secondary antibody Streptavidin-APC-Cy7 (1:100, eBioscience) was used, followed by the addition of 7-amino-actinomycin D (7-AAD, 1:20, eBioscience) to discriminate the dead cells. Mouse club and AT2 cells were sorted based on their surface expression pattern, $CD31^{-}CD34^{-}CD45^{-}EpCAM^{+}CD24^{+}Sca\text{-}1^{+}$ and $CD31^{-}CD34^{-}CD45^{-}EpCAM^{+}CD24^{-}Sca\text{-}1^{-}$, respectively.

Transmission electron microscope

Mouse club or AT2 cells were sorted by FACS as described above. Then the cells were placed in the electron microscope fixing solution (pH7.0–7.5) (Servicebio, Wuhan, China) containing 2.5% glutaraldehyde, and fixed at 4°C for 2 h. Phosphate buffer (0.1M) (pH=7.4) was used to wash the cells 3 times (15 min each). Starvation acid (1%) was used for post-fix, keeping away from light for 2 h. Then, the cells were washed 3 times with 0.1M phosphate buffer (15 min each). The samples were dehydrated at room temperature as the following: 30%, 50%, 70%, 80% and 95% ethanol for 20 min, 100% ethanol twice (20 min each) and acetone twice (15 min each). For resin penetration and embedding, the samples were sequentially treated with alcohol/EMBed 812 (1:1) for 2–4 h, acetone/EMBed 812 (1:2) overnight, and pure EMBed 812 for 5–8 h at 37°C. The samples were maintained in the pure EMBed 812 at 37°C overnight. The embedding board was placed in 60°C oven for 48 h to polymerize. Ultrathin sections (60–80 nm) were made and mounted on cuprum grids. Cuprum grids were stained using 2% uranium acetate saturated alcohol solution avoiding light for 8 min, rinsed in 70% ethanol and ultra-pure water for 3 times each. Then the samples were treated by 2.6% lead citrate avoiding CO_2 for 8 min, and rinsed with ultra-pure water 3 times. Cuprum grids were dried overnight at room temperature. Electron microscope (Tecnai G2 F20, FEI, Eindhoven, Holland) was used to observe and image.

Organoid cultures

FACS-sorted mouse club cells (5×10^3) or AT2 cells (2×10^4) were co-cultured with MLg (2×10^5), mouse lung fibroblast cells (ATCC, Rockefeller, MD, USA), in Matrigel/culture medium (1:1) respectively. The culture medium included Dulbecco's modified Eagle Medium/F12 (Corning, Corning, NY, USA), 1% insulin/transferrin/selenium (Sigma), 10% FBS, 100 IU/ml penicillin, 100 μg/ml streptomycin, and 10 μM SB431542 (Sigma). In the treatment group, 10 μM HCQ was added to the culture medium. Then, the mixture was transferred to the Transwell inserts in 24-well plates (Corning) containing the culture medium at the bottom. An incubator with a humidified 37°C with 5% CO_2 was used to maintain cultures, and the culture medium was changed every other day. The organoids were imaged using an inverted fluorescence microscope (Olympus, Tokyo, Japan). The colony-forming efficiency (CFE) was calculated as the number of organoids (greater than 50 μm in diameter) in each insert as a percentage of seeded epithelial cells.

Assay for the viability of AT2 and club cells

Club cells (1×10^4 cells/well) or AT2 cells (2×10^4 cells/well) were plated in a 96-well plate (Labgic, Beijing, China). Serially diluted compounds were added in quadruplicate and incubated at 37°C for 24 h. Thereafter, according to the manufacturer's instructions,3-(4,5-dimethylthiazol-2-yl)-5-(3-carboxymethoxyphenyl)-2-(4-sulfophenyl)-2H-tetrazolium (MTS) was directly added to the culture wells to evaluate the effect of each compound on the viability of club or AT2 cells at 490 nm wavelength on a Spectrophotometer (Multiskan GO, Thermo Fisher Scientific, Vantaa, Finland).

RNA isolation and quantitative real-time PCR (qPCR)

Total RNA was extracted from organoid cultures and mouse lung tissues using TRIzol reagent (Invitrogen, Carlsbad, CA, USA), according to the manufacturer's instructions. RNA was reverse transcribed using SuperScript III reagents with oligo-d (T) (Invitrogen) and random hexamer primers (Takara, Tokyo, Japan). qPCR was performed with specific primers using SYBR green supermix (Vazyme, Nanjing, China) in the Light Cycler 96 (Roche, Nutley, NJ, USA) Real-Time PCR system under the following conditions: 95°C for 2 min, 95°C for 10 s, 40 cycles of 60°C for 20 s, and 72°C for 20 s. The relative expression level of each gene of interest was normalized to that of *Actb* in the same sample. The following primers (Sangon Biotech) were used for qRT-PCR: *Actb F*: 5'-GGCCAACCGTGAAAAGATGA-3', *Actb* -R: 5'-CAGCCTGGATGGCTACGTACA-3'; *Cyp2f2*-F: 5'-CGACTGCTTCCTCACAAAGA-3', *Cyp2f2*-R: 5'-GTCATCAGCAGGGTATCCATATT-3'; *Foxa3*-F: 5'-CTTGGTGGAGGTTGGGTGAG-3'; *Foxa3*-R: 5'-ACAGGCAGTATTCCCAAGCC-3'; Tubulin-F: 5'-GGTGATGTGGTTCCCAAAGA-3'; Tubulin-R: 5'-GTGGGAGGCTGGTAGTTAATG-3'; *Foxj1*-F: 5'-AGAGAGTGAGGG CAAGAGAC-3', *Foxj1*-R: 5'-GCGGGCTTAGAGACCA TTTC-3'; *Clca1*-F: 5'-GGCATCGTCATCGCCATAG-3', *Clca1*-R: 5'-CACCATGTCCTTTATGTGTTGAATG-3'; *Sftpc*-F: 5'-GAAGATGGCTCCAGAGAGCATC-3', *Sftpc*-R 5'-GGACTCGGAACCAGTATCATGC-3'; *Pdpn*-F: 5'-TGCTACTGGAGGGCTTAATGA-3', *Pdpn*-R: 5'-TGCTGAGGTGGACAGTTCCT-3'; *Aqp5*-F: 5'-GGTGGTCATGAATCGGTTCAGC-3', *Aqp5*-R: 5'-GTCCTCCTCTGGCTCATATGTG-3'; *Fn1*-F: 5'-GTGTAGCACAACTCCAATTACGAA-3'; *Fn1*-R: 5'-GGAATTTCCGCCTCGAGTCT-3'; *Collagen 1*(*Col1*)-F: 5'-CCAAGAAGACATCCCTGAAGTCA-3'; *Col1*-R: 5'-TGCACGTCATCGCACACA-3'.

Immunofluorescence

Immunofluorescence was conducted as described previously [21]. Briefly, lung tissue was perfused and fixed with formalin. Organoid cultures were embedded in O.C.T. compound. Lung tissue or organoid sections were blocked with 5% BSA (Boster, Wuhan, China) and incubated with anti-Ki67 (1:200, eBioscience), anti-CCSP (1:1,000; Santa Cruz Biotechnology, Dallas, TX, USA), anti-CYP2F2 (1:100; Santa Cruz Biotechnology), anti-ACT (1:200; Sigma), anti-CLCA1 (1:200; Abcam, Cambridge, UK), and pro-SPC (1:200, Millipore, Boston, MA, USA). Thereafter, a fluorescent-coupled secondary antibody (1:200, Invitrogen) was added, and the nuclei were stained with Fluromount G containing 4'-6'-diamidino-2-phenylindole (DAPI). The stained sections were imaged using an IX73 inverted fluorescent microscope (Olympus).

Hematoxylin and eosin (H&E) staining

H&E staining was conducted as described previously [21]. Briefly, lung sections were deparaffinized and rehydrated for hematoxylin and eosin staining (Solarbio). Thereafter, 95% alcohol and 100% alcohol solutions were used for dehydration (5 min each). The glass slides containing the sections were sealed with neutral resin.

Masson trichrome staining

Masson trichrome staining was performed as previously described [21]. Briefly, paraffin-embedded lung tissue sections were treated with Masson's compound staining solution, phosphomolybdic acid dye, aniline blue, and differentiation solution (MXB, Fuzhou, China). After dehydration, the sections were sealed with neutral balsam for imaging.

Statistical analysis

All data are presented as mean ± SD. The sample size was based on the previous studies[38–40]. No animals were excluded for data analysis. Every experiment were repeated two or more times. One-way ANOVA and Student's *t*-test were performed to determine *P*-values. Statistical significance was defined as $P<0.05$ (*$P<0.05$; ** $P<0.01$).

Results

HCQ does not affect the viability of mouse club and AT2 cells

HCQ is clinically used as an antiviral drug to treat patients with COVID-19 [41–43]. However, it is unknown whether HCQ has a negative influence on the regenerative capability of lung epithelial stem cells dur-

ing the suppression of virus activity. Therefore, we explored the influence of HCQ on the regenerative ability of club and AT2 cells. FACS was used to fractionate the mouse lung epithelial stem/progenitor cells. Thereafter, single-cell suspensions of lung tissue from C57BL/6 mice were obtained by immunostaining with fluorescent-labeled antibodies against cell surface markers and reactive dyes. Epithelial cells were isolated by selecting EpCAM^{pos}, CD31^{neg}, CD34^{neg}, and CD45^{neg} cells. Mouse club and AT2 cells were further separated by CD24 and Sca-1 staining (Fig. 1A). We oberved that the autofluorescence of club cells was stronger than that of AT2 cells in mice (Fig. 1B). Immunofluorescence staining with anti-CCSP- or anti-pro-SPC antibodies proved the char-

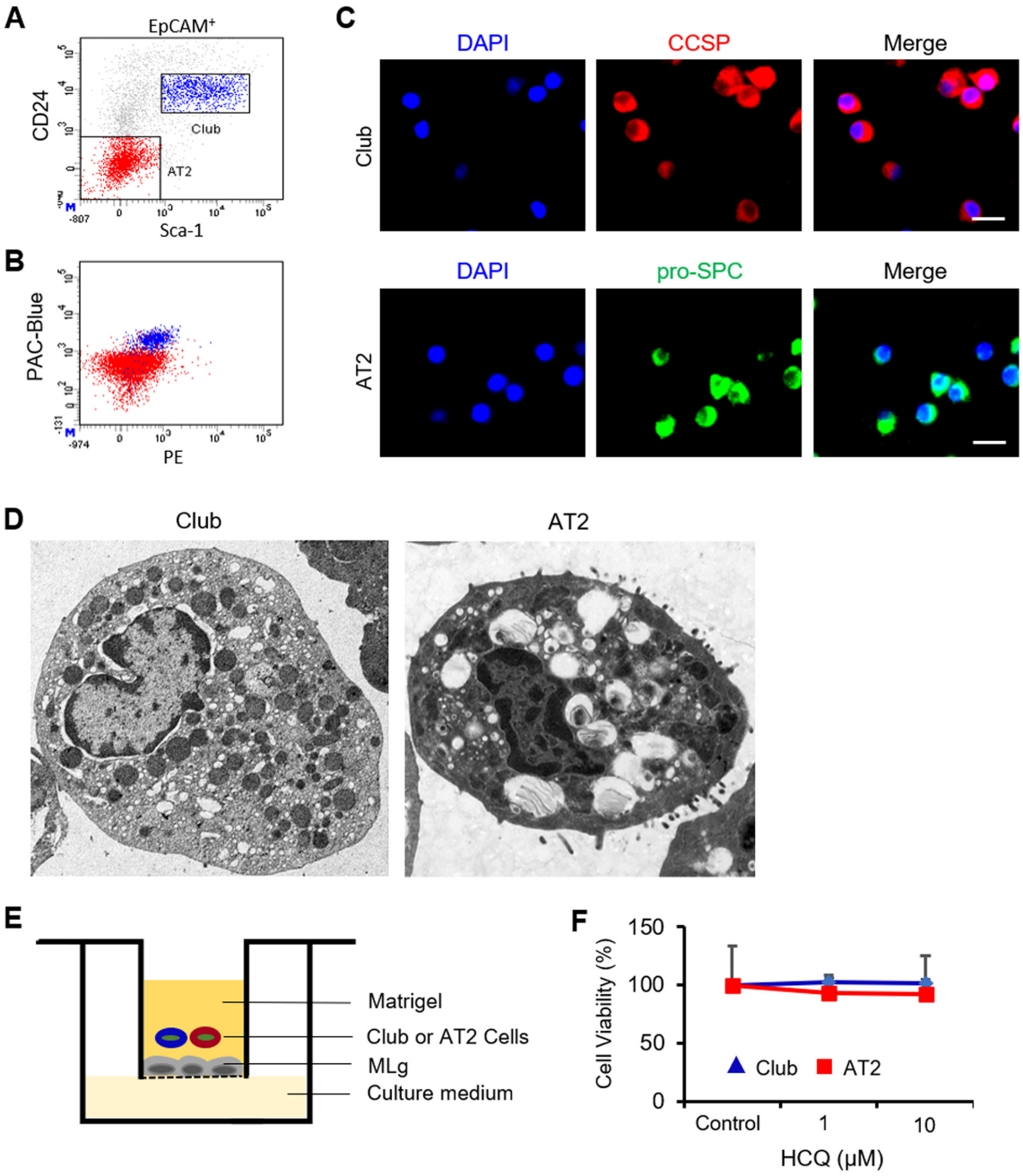

Fig. 1. Isolation and organoid cultures of lung epithelial progenitor cells. (A) Lung epithelial progenitor cells, including club and AT2 cells, were retrieved from normal mice by fluorescent activated cell sorting. (B) The autofluorescence intensity of club and AT2 cells were detected using fluorescence-activated cell sorting. (C) Immunofluorescence staining of club and AT2 cells with CCSP and SPC, respectively. Scale bar=10 μm. (D) Transmission electron microscopy images of club and AT2 cells. (E) Club or AT2 cells were cultivated in transwell chambers with MLg cells to establish an organoid platform. (F) MTS analysis was used to derive the cytotoxicity of hydroxychloroquine (HCQ) in mouse club and AT2 cells (n=4). Data are expressed as mean ± SD. Statistical significance was determined using one-way ANOVA.

 doi: 10.1538/expanim.21-0168

acteristics of sorted mouse club and AT2 cells (Fig. 1C). Morphologically, transmission electron microscopy indicated that club cells exhibit a round shape with an abundance of cytoplasm and organelles, while AT2 cells exhibit a columnar shape with a rounded nucleus and lamella bodies (Fig. 1D). The sorted mouse club or AT2 cells were cultivated with MLg cells in transwell chambers to establish an organoid culture system (Fig. 1E). MTS was used to evaluate the cytotoxicity of HCQ. Based on the MTS analysis, the viability of mouse club cells and AT2 cells was not affected by HCQ at a concentration of 10 μM or lower (Fig. 1F).

Effects of HCQ on the *in vitro* regenerative ability of mouse club cells

To determine whether HCQ affects the regenerative function of club cells *in vitro*, we adopted the established 3-D organoid-based system. Herein, we found that HCQ increased the CFE of club cells; however, its effect on the size of club cell-derived organoids was negligible (Figs. 2A and B). We also measured the mRNA expression of the differentiation-related genes in colonies derived from club cells and found that ciliated cells (*Foxj1*) and goblet cells (*Clca1*) differentiating from club cells were both increased (Fig. 2C). Furthermore, after immunofluorescence staining and quantification of the fraction of Ki67$^+$CYP2F2$^+$ cells in total pro-CYP2F2$^+$ cells in organoid colonies, we found that HCQ did not affect the proliferation of club cells in organoid colonies (Figs. 2D and E). These findings indicate that HCQ promotes the differentiation of club cells but has no significant effect on their proliferation.

HCQ does not impair the regenerative ability of mouse club cells after airway epithelial injury

To explore the effect of HCQ on club cell regeneration *in vivo*, we adopted a naphthalene-induced airway injury model. Intraperitoneal injection of naphthalene selectively eliminates airway club cells[44]. HCQ was intraperitoneally administered daily starting on day one after naphthalene injection, and the mouse lung tissues were collected on D7 and D14, respectively (Fig. 3A). HCQ, at dosage of either 10 mg/kg or 50 mg/kg, did not affect the expression of *Clca1*, *Foxa3*, *Foxj1*, Tubulin in

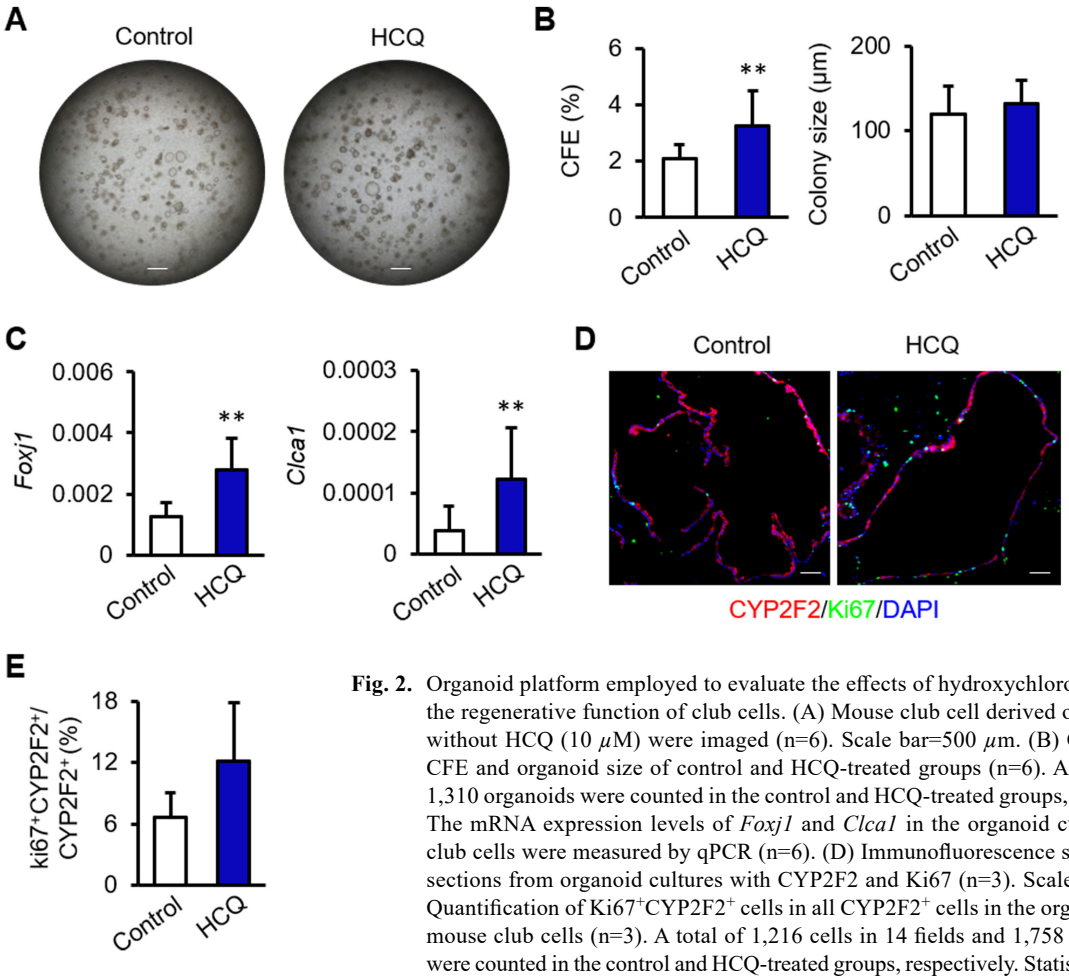

Fig. 2. Organoid platform employed to evaluate the effects of hydroxychloroquine (HCQ) on the regenerative function of club cells. (A) Mouse club cell derived organoids with or without HCQ (10 μM) were imaged (n=6). Scale bar=500 μm. (B) Quantification of CFE and organoid size of control and HCQ-treated groups (n=6). A total of 696 and 1,310 organoids were counted in the control and HCQ-treated groups, respectively. (C) The mRNA expression levels of *Foxj1* and *Clca1* in the organoid cultures of mouse club cells were measured by qPCR (n=6). (D) Immunofluorescence staining of frozen sections from organoid cultures with CYP2F2 and Ki67 (n=3). Scale bar=50 μm. (E) Quantification of Ki67$^+$CYP2F2$^+$ cells in all CYP2F2$^+$ cells in the organoid cultures of mouse club cells (n=3). A total of 1,216 cells in 14 fields and 1,758 cells in 23 fields were counted in the control and HCQ-treated groups, respectively. Statistical significance of all data was calculated by two-tailed Student's *t*-test. $^{**}P<0.01$.

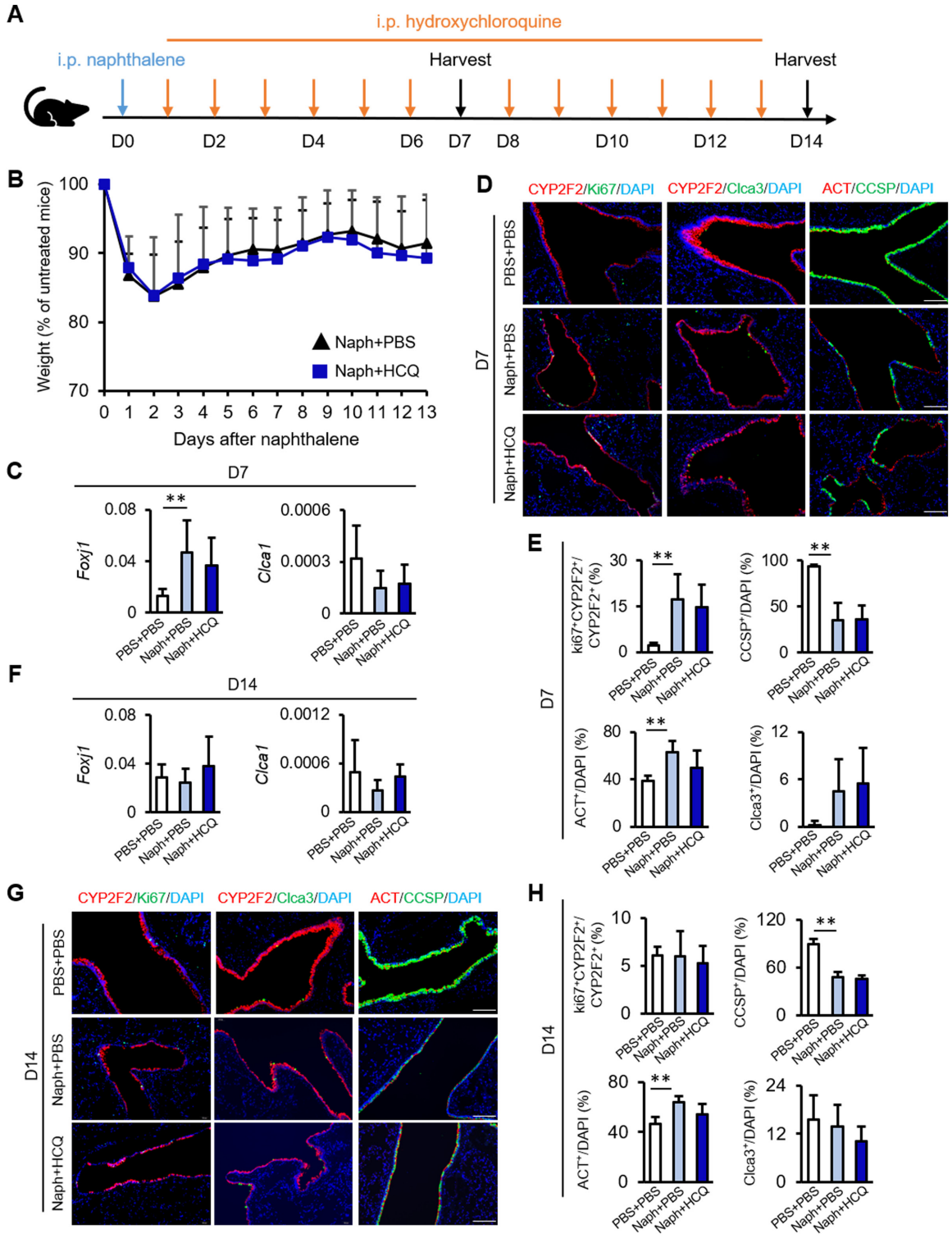

Fig. 3. Hydroxychloroquine (HCQ) had no effect on the regeneration of mouse club cells during naphthalene-induced airway epithelial injury. (A) Schematic diagram of naphthalene-induced airway injury and the administration of HCQ (50 mg/kg per day) to mice. (B) Body weight of mice was recorded during naphthalene-induced mouse airway injury (n=8). (C) qPCR analysis of *Foxj1* and *Clca1* mRNA expression in mouse lung at 7 days after naphthalene injury (n=8). (D) Immunofluorescence staining of lung sections at 7 days after naphthalene injury (n=8). Scale bar=50 μm. (E) Quantification of club, ciliated, and goblet cells at 7 days after naphthalene injury (n=8). A total of 17,098 cells in 44 fields, 17,067 cells in 99 fields and 16,093 cells in 110 fields were counted in the PBS+PBS group, Naph+PBS-treated and Naph+HCQ-treated groups, respectively. (F) qPCR analysis of *Foxj1* and *Clca1* mRNA expression in mouse lung at 14 days after naphthalene injury (n=8). (G) Immunofluorescence staining of lung sections at 14 days after naphthalene injury (n=8). Scale bar=50 μm. (H) Quantification of club, ciliated, and goblet cells during naphthalene injury in the absence or presence of HCQ (n=8). A total of 17,343 cells in 51 fields, 20,888 cells in 91 fields and 11,143 cells in 60 fields were counted in the PBS+PBS group, Naph+PBS-treated and Naph+HCQ-treated groups, respectively. Statistical significance of all data was determined calculated using one-way ANOVA. ** P<0.01.

the lung at day 7 or day 14 after naphthalene injection (Supplementary Figs. 1A, B, and Fig. 3). Compared with Naph+PBS group, *Cyp2f2* expression was increased in Naph+HCQ (10 mg/kg) group at day 14 after naphthalene (Supplementary Fig. 1B). The higher dose (50 mg/kg) was chosen to further investigate possible effects of HCQ on airway epithelial stem cell function. As expected, body weight was reduced following naphthalene administration, however, body weight recovery began on day three (Fig. 3B). No difference was observed in body weights between the PBS-treated and HCQ-treated groups throughout the treatment period (Fig. 3B). At day 7 after naphthalene injury, *Foxj1* expression was up-regulated in the lung as compared to non-injury group (Fig. 3C). Immunofluorescence staining indicated that naphthalene caused a significant decrease in the abundance of CCSP-expressing club cells, while increase in acetylated tubulin (ACT)-expressing ciliated cells as compared to non-injured group (Figs. 3D and E). In addition, the quantitative statistics showed that, at this timpoint, the $Ki67^{+}CYP2F2^{+}/CYP2F2^{+}$ ratio was significantly higher in Naph+PBS group than that in the PBS+PBS group (Fig. 3E). However, HCQ did not affect the abundance of CCSP-expressing club, ACT-expressing ciliated or Clca3-expressing goblet cells during naphthalene-induced airway epithelial injury (Figs. 3D and E). Likewise, at day 14 after naphathalene injury, HCQ exhibited no effects on the mRNA expression of *Foxj1* and *Clca1*, or abundance of club cells, ciliated cells or goblet cells during naphthalene injury (Figs. 3F–H, and Supplementary Fig. 1B). These findings indicated that naphthalene injury can significantly reduce club cells and increase ciliated cells, but HCQ does not affect the proliferation and differentiation of mouse club cells *in vivo*.

Effects of HCQ on the *in vitro* regenerative ability of mouse AT2 cells

The organoids derived from mouse AT2 cells revealed that HCQ decreased the CFE of mouse AT2 cells but increased the colony size (Figs. 4A and B). Furthermore, based on quantitative PCR analysis of AT2 cell-derived organoid cultures, the expression levels of *Pdpn* and *Aqp5*, markers of AT1 cells, didn't have obvious difference between the HCQ and control groups (Fig. 4C). Immunofluorescence staining of mouse lung tissues suggested that there was no difference in AT2 cell proliferations between the control group and the HCQ treatment group at this time *in vitro* (Fig. 4D).

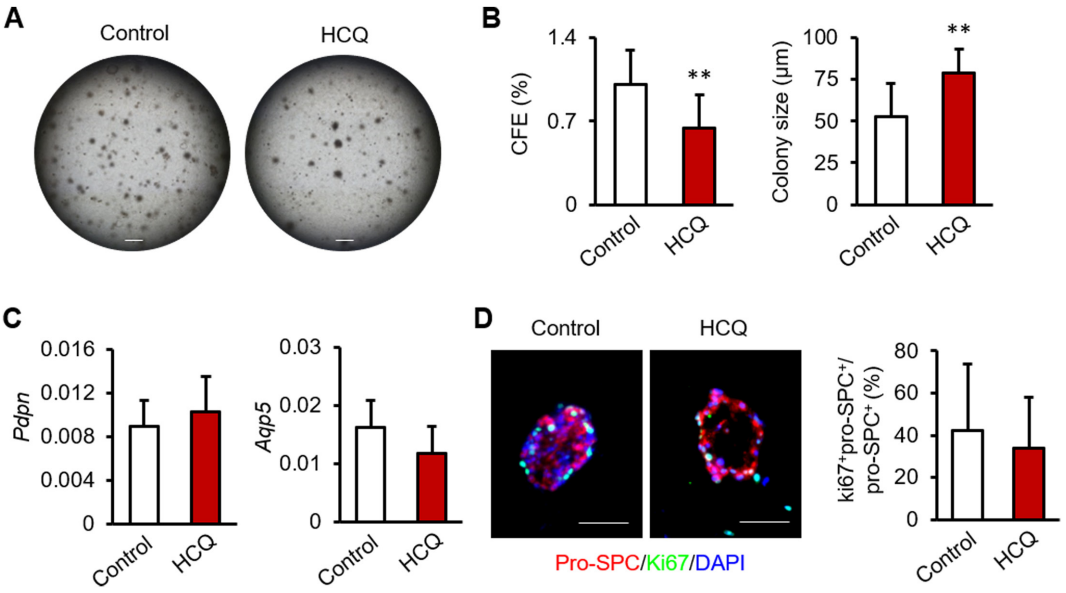

Fig. 4. Organoid model derived to evaluate the effects of hydroxychloroquine (HCQ) on the regenerative function of mouse AT2 cells. (A) Organoids derived from AT2 cells cultured with or without HCQ (10 μM) were imaged (n=9). Scale bar=500 μm. (B) CFE and size of the organoids derived from mouse AT2 cells cultured with or without HCQ (n=9). A total of 1,046 and 747 organoids were counted in the control and HCQ-treated groups, respectively. (C) The expression levels of *Pdpn* and *Aqp5* in the organoid cultures of AT2 cells were measured using qPCR (n=6). (D) Immunofluorescence staining of the organoid cultures with pro-SPC and Ki67, and quantification of $Ki67^{+}$AT2 cells in all AT2 cells in the organoid cultures of AT2 cells (n=3). A total of 619 cells in 12 fields and 625 cells in 16 fields were counted in the control and HCQ-treated groups, respectively. Scale bar=50 μm. Statistical significance of all data was calculated by two-tailed Student's *t*-test, $^{**}P<0.01$.

HCQ does not affect the regenerative ability of mouse AT2 cells during BLM-induced alveolar epithelial injury

To evaluate the possible effect of HCQ on AT2 cell regeneration *in vivo*, we employed a BLM-induced alveolar epithelial injury mouse model. Bleomycin is known to injure AT2 and AT1 cells [44]. After the induction of injury, HCQ was intraperitoneally administered daily starting on day 1 after BLM injection (Fig. 5A). Mice were then sacrificed on day 7 or 14 for analysis (Fig. 5A). HCQ, at dosage of either 10 mg/kg or 50 mg/kg, did not affect the expression of *Sftpc*, *Pdpn*, *Aqp5*, *Fn1* or *Col1* in the lung at day 7 or day 14 after BLM (Supplementary Figs. 2A, B, and Fig. 5). The higher dose (50 mg/kg) was chosen for the following experiments to maximize possible effects of HCQ on alveolar epithelial stem cell function. Injury compelled mice to lose weight, however, body weight began to recover after day 7 (Fig. 5B). No difference in body weight was found between the HCQ and control groups over the entire injury process (Fig. 5B). At day 7 after BLM-induced injury, Masson and H&E staining of the lung tissues indicated that the alveolar structure was injured (Fig. 5C). The mRNA expression of *Fn1* and *Col1* in lung tissue of mice increased significantly (Fig. 5D). And *Sftpc* and *Aqp5* gene expression levels were decreased at this time point (Fig. 5E). As compared to the BLM+PBS group, HCQ exhibited no effects on bleomycin-induced alveolar injury, the expression of these alveolar epithelial genes or fibrotic genes, or proliferative potential of AT2 cells at this time point (Figs. 5C–F, and Supplementary Fig. 2A). Compared to the lung tissue harvested at day 7, more severe damage was observed in the tissues retrieved at day 14, which was related to the development of lung fibrosis (Fig. 5G). At day 14 after BLM, the mRNA expression of *Fn1* and *Col1* in lung tissue of mice remained increased as compared to non injury group (Fig. 5H). However, compared to the BLM+PBS group, HCQ didn't effect the mRNA expression of *Fn1* and *Col1* in lung tissue (Fig. 5H). Similar to the results at day 7, HCQ exhibited no effects on bleomycin-induced alveolar injury, the expression of fibrotic genes and epithelial markers at day 14 after BLM (Figs. 5G–I, and Supplementary Fig. 2B). In addition, immunofluorescence analysis confirmed that HCQ did not affect the proliferation of AT2 cells at day 14 after BLM (Fig. 5J).The findings showed BLM caused collagen deposition, fibrosis and compensatory alveolar epithelial cell proliferation in mouse lung tissue, but HCQ exhibits a limited role in regulating the regenerative ability of AT2 cells after bleomycin treatment.

Discussion

There is an urgent need to not only develop anti-SARS-CoV-2 drugs but also establish platforms to screen drug candidates that do not impair lung regeneration as lung epithelial stem/progenitor cells, including airway club cells and alveolar AT2 cells, are injured by SARS-CoV-2. In this study, we adopted a 3-D lung organoid platform and lung epithelial injury repair mouse models to assess the effects of HCQ on lung epithelial regeneration. Serum HCQ levels were reported to range from 0–7.9 μM in patients according to a weight-based dosing of 6.5 mg/kg [45, 46]. Further, the 50% maximal effective concentration (EC50) of HCQ was found to range from 4.06–12.96 μM in VeroE6 cells [6]. In order to be relevant to clinic, we selected HCQ at 10 μM for *in vitro* organoid cultures, and HCQ at 10 or 50 mg/kg for the lung injury mouse models.

The organoid platform indicated that HCQ enhances the colony-forming ability and differentiating ability of goblet and ciliated cells of mouse club cells without affecting their proliferation. However, these effects were abolished during naphthalene-induced airway epithelial injury *in vivo*. Although HCQ appeared to inhibit the colony-forming ability of mouse AT2 cells *in vitro*, the regenerative and differentiation abilities of AT2 cells were unaffected by HCQ during BLM-induced alveolar epithelial injury *in vivo*. In our previous study, we demonstrated that CQ (Chloroquine) does not affect the proliferation and differentiation of mouse club and AT2 cells [38]. CQ and HCQ share similar chemical structures and mechanisms of action as weak bases and immunomodulators [47]. CQ is metabolized into desethylchloroquine, whereas HCQ is metabolized into desethylchloroquine and desethylhydroxychloroquine [48]. Therefore, different metabolic products may contribute to the discrepancy in the different effects of CQ and HCQ on lung stem/progenitor cell function in *in vitro* organoid cultures. The effects of HCQ on the function of the mouse club and AT2 cells were found to be abolished in mouse models. Such finding suggests that the *in vivo* environment could compensate for the HCQ-induced effects on lung epithelial stem/progenitor cells. Such a dicrepancy in the findings between organoids and lung injury mouse models reminds us of the strengths and limitations of drug screening models.

Recently, rising organoid technology has investigated the direct role of drugs on lung stem/progenitor cells that can be gained from animals or human subjects. We previously adopted an organoid model to evaluate the direct role of several anti-SARS-CoV-2 drug candicates [38]. Lung organoids can be used to model human lung biol-

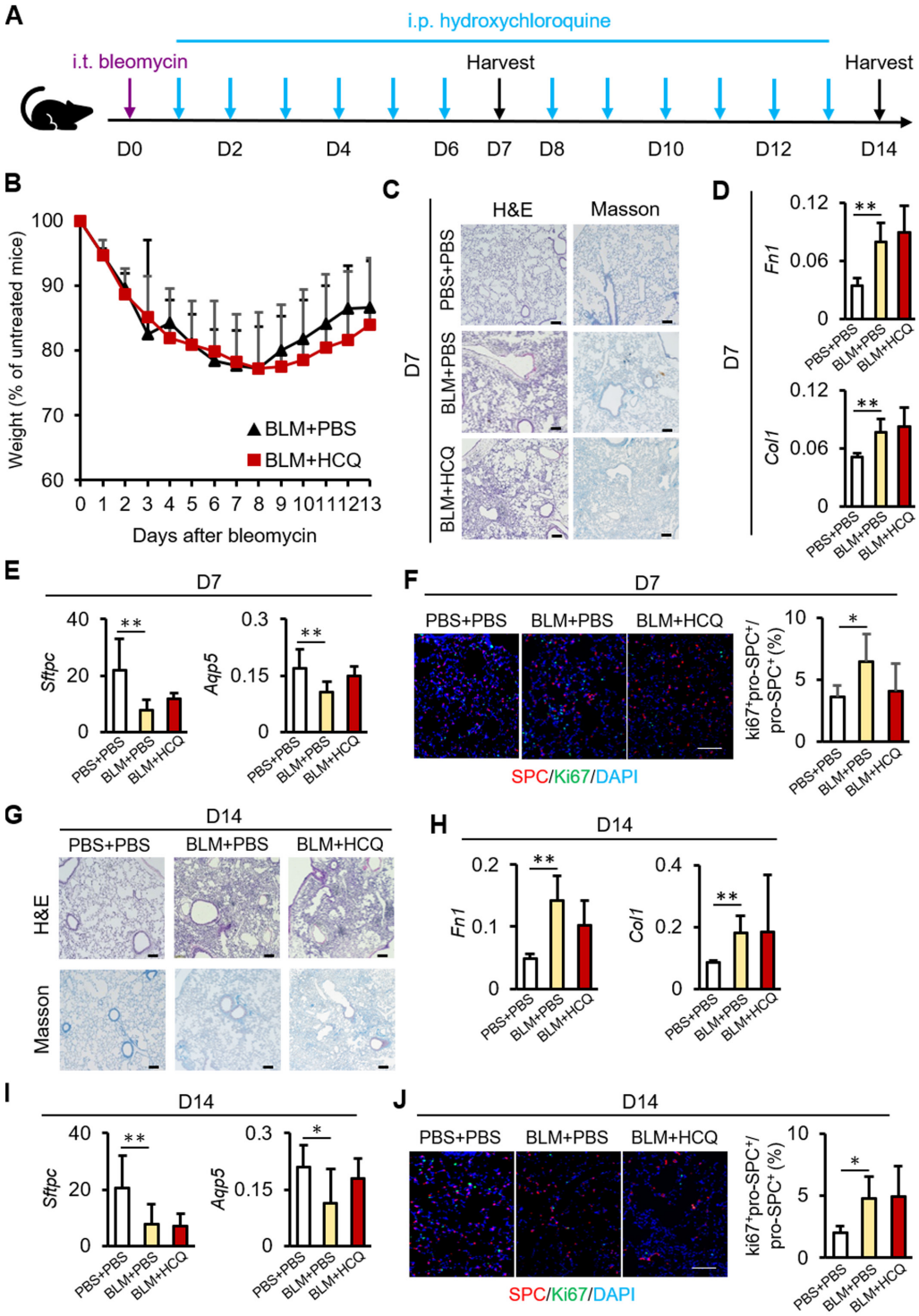

Fig. 5. Hydroxychloroquine (HCQ) had no effect on the regeneration of AT2 during bleomycin (BLM)-induced alveolar epithelial injury. (A) Schematic diagram of the induction of mouse alveolar epithelial injury by BLM and the administration of HCQ (50 mg/kg per day). (B) Body weight of mice was recorded during BLM-induced mouse alveolar injury (n=10). (C) Hematoxylin and eosin staining and Masson trichrome staining of the lung sections at day 7 after BLM (n=10). Scale bar=100 μm. (D) mRNA expression of *Fn1* and *Col1* were determined in mouse lung tissues at day 7 after BLM (n=10). (E) qPCR analysis of *Sftpc* and *Aqp5* mRNA expression in mouse lung at 7 days after BLM injury (n=8). (F) Immunofluorescent staining and quantitative analysis of AT2 cell proliferation at day 7 after BLM injury (n=8). A total of 5,337 cells in 25 fields, 711 cells in 20 fields and 1,293 cells in 29 fields were counted in the PBS+PBS group, BLM+PBS-treated and BLM+HCQ-treated groups, respectively. Scaled bar=50 μm. (G) Hematoxylin and eosin staining and Masson trichrome staining of the lung sections at day 14 after BLM (n=10). Scale bar=100 μm. (H) mRNA expression of *Fn1* and *Col1* were determined in mouse lung tissues at day 14 after BLM (n=10). (I) qPCR analysis of *Sftpc* and *Aqp5* mRNA expression in mouse lung at 14 days after BLM injury (n=8). (J) Immunofluorescent staining and quantitative analysis of AT2 cell proliferation at day 14 after BLM injury (n=8). A total of 5,178 cells in 25 fields, 931 cells in 28 fields and 931 cells in 27 fields were counted in the PBS+PBS group, BLM+PBS-treated and BLM+HCQ-treated groups, respectively. Scaled bar=50 μm. Statistical significance of all data was calculated using one-way ANOVA. **P*<0.05, ***P*<0.01.

ogy using human pulmonary epithelial cells [38]. To date, human proximal airway and distal alveolar organoids have been successfully derived [49, 50]. Lung organoids can model the developmental process of the lung, as well as recapitulate the 3-D essential structural (such as alveolars, airways, and lung buds) and functional aspects of the lung *in vitro* [47]. However, there is a lack of key *in vivo* characteristics such as a defined body axis, nervous system and functional immune system, functional vasculature, and force change during gas exchange in organoids [51]. In addition, HCQ is metabolized in the liver into desethylchloroquine and desethylhydroxychloroquine, which then circulates to the lungs [48]. Acting ingredients may have different regulatory roles from those of prodrugs. Mouse lung injury models have all these elements, but the physical differences between mice and humans create a major obstacle in translational medicine [52]. In this study, we were unable to access human lung tissues for airway and alveolar epithelial progenitor cells. We propose that the combination of organoid cultures with human cells and mouse lung injury models would be a solution to identify lung regeneration-friendly drugs for COVID-19 treatment. Combining the *in vitro* and *in vivo* findings, we concluded that HCQ has a limited effect on the regenerative ability of lung epithelial stem/progenitor cells, reducing the concern of potential fibrotic progression in recovered COVID-19 patients administered HCQ.

Author Contributions

These authors contributed equally: F.Z., J.W., Q. Wang, Z.H., and Y.Z; Corresponding author, Q. Wu, H.C.; Conceptualization, Q. Wu and H.C.; Investigation, F.Z., J.W., and Q.Wang; Formal Analysis, F.Z., J.W., Q. Wang, Z.H., Y.Z., X.L., Q.Wu, and H.C.; Data Curation, F.Z., J.W., Q. Wang, Z.H., and Y.Z; Writing—Original Draft Preparation, F.Z., J.W., Q.Wang, Z.H., Y.Z., and H.C.; Writing—Review & Editing, F.Z., J.W., Q.Wang, Z.H., Y.Z., X.L., Q.Wu, and H.C.; Supervision, Q.Wu and H.C.; Project Administration, H.C. All authors have read and agreed to the published version of the manuscript.

Funding

This study was supported by the National Natural Science Foundation of China (81773394, 81970001, 82070001, and 82100077); the Natural Science Foundation of Tianjin (20JCQNJC01790 and 18ZXDBSY00150); the Science and Technology Planning Project of Tianjin Jinnan District (20200118); and the Haihe Hospital Fund of China (HHYY-202008). The funders had no role in the study design, data collection and analysis, decision to publish, or preparation of the manuscript.

Institutional Review Board Statement

This study was approved by the Ethics Committee of Haihe Hospital, Tianjin University (ethical approval number: 2020HHSQKT-047).

Conflicts of Interest

The authors declare that there is no conflict of interest.

Data Availability Statement

The authors declare that all the data supporting the findings of this study are available within the article and its supplementary Information files and from the corresponding authors on reasonable request.

References

1. Umakanthan S, Sahu P, Ranade AV, Bukelo MM, Rao JS, Abrahao-Machado LF, et al. Origin, transmission, diagnosis and management of coronavirus disease 2019 (COVID-19). Postgrad Med J. 2020; 96: 753–758. [Medline]
2. Singhal T. A Review of Coronavirus Disease-2019 (COVID-19). Indian J Pediatr. 2020; 87: 281–286. [Medline] [CrossRef]
3. Zhang H, Zhou P, Wei Y, Yue H, Wang Y, Hu M, et al. Histopathologic Changes and SARS-CoV-2 Immunostaining in the Lung of a Patient With COVID-19. Ann Intern Med. 2020; 172: 629–632. [Medline] [CrossRef]
4. Schaefer IM, Padera RF, Solomon IH, Kanjilal S, Hammer MM, Hornick JL, et al. In situ detection of SARS-CoV-2 in lungs and airways of patients with COVID-19. Mod Pathol. 2020; 33: 2104–2114. [Medline] [CrossRef]
5. Basil MC, Katzen J, Engler AE, Guo M, Herriges MJ, Kathiriya JJ, et al. The Cellular and Physiological Basis for Lung Repair and Regeneration: Past, Present, and Future. Cell Stem Cell. 2020; 26: 482–502. [Medline] [CrossRef]
6. Liu J, Cao R, Xu M, Wang X, Zhang H, Hu H, et al. Hydroxychloroquine, a less toxic derivative of chloroquine, is effective in inhibiting SARS-CoV-2 infection in vitro. Cell Discov. 2020; 6: 16. [Medline] [CrossRef]
7. Whitsett JA. Airway Epithelial Differentiation and Mucociliary Clearance. Ann Am Thorac Soc. 2018; 15:(Suppl 3): S143–S148. [Medline] [CrossRef]
8. Wu A, Song H. Regulation of alveolar type 2 stem/progenitor cells in lung injury and regeneration. Acta Biochim Biophys Sin (Shanghai). 2020; 52: 716–722. [Medline] [CrossRef]
9. Kanagaki S, Ikeo S, Suezawa T, Yamamoto Y, Seki M, Hirai T, et al. Directed induction of alveolar type I cells derived from pluripotent stem cells via Wnt signaling inhibition. Stem Cells. 2021; 39: 156–169. [Medline] [CrossRef]
10. Kreutz R, Algharably EAE, Azizi M, Dobrowolski P, Guzik T, Januszewicz A, et al. Hypertension, the renin-angiotensin system, and the risk of lower respiratory tract infections and lung injury: implications for COVID-19. Cardiovasc Res. 2020; 116: 1688–1699. [Medline] [CrossRef]

11. Lukassen S, Chua RL, Trefzer T, Kahn NC, Schneider MA, Muley T, et al. SARS-CoV-2 receptor ACE2 and TMPRSS2 are primarily expressed in bronchial transient secretory cells. EMBO J. 2020; 39: e105114. [Medline] [CrossRef]
12. George PM, Wells AU, Jenkins RG. Pulmonary fibrosis and COVID-19: the potential role for antifibrotic therapy. Lancet Respir Med. 2020; 8: 807–815. [Medline] [CrossRef]
13. Xu J, Xu X, Jiang L, Dua K, Hansbro PM, Liu G. SARS-CoV-2 induces transcriptional signatures in human lung epithelial cells that promote lung fibrosis. Respir Res. 2020; 21: 182. [Medline] [CrossRef]
14. Lamers MM, van der Vaart J, Knoops K, Riesebosch S, Breugem TI, Mykytyn AZ, et al. An organoid-derived bronchioalveolar model for SARS-CoV-2 infection of human alveolar type II-like cells. EMBO J. 2021; 40: e105912. [Medline] [CrossRef]
15. Mulay A, Konda B, Garcia G Jr, Yao C, Beil S, Villalba JM, et al. SARS-CoV-2 infection of primary human lung epithelium for COVID-19 modeling and drug discovery. Cell Rep. 2021; 35: 109055. [Medline] [CrossRef]
16. Rackley CR, Stripp BR. Building and maintaining the epithelium of the lung. J Clin Invest. 2012; 122: 2724–2730. [Medline] [CrossRef]
17. Karagiannis TC, Li X, Tang MM, Orlowski C, El-Osta A, Tang ML, et al. Molecular model of naphthalene-induced DNA damage in the murine lung. Hum Exp Toxicol. 2012; 31: 42–50. [Medline] [CrossRef]
18. Tolbert JR, Kabali P, Brar S, Mukhopadhyay S. An accuracy aware low power wireless EEG unit with information content based adaptive data compression. Annu Int Conf IEEE Eng Med Biol Soc. 2009; 2009: 5417–5420. [Medline]
19. Hsu HS, Liu CC, Lin JH, Hsu TW, Su K, Hung SC. Repair of naphthalene-induced acute tracheal injury by basal cells depends on β-catenin. J Thorac Cardiovasc Surg. 2014; 148: 322–332. [Medline] [CrossRef]
20. Della Latta V, Cecchettini A, Del Ry S, Morales MA. Bleomycin in the setting of lung fibrosis induction: From biological mechanisms to counteractions. Pharmacol Res. 2015; 97: 122–130. [Medline] [CrossRef]
21. Li X, Wu J, Sun X, Wu Q, Li Y, Li K, et al. Autophagy Reprograms Alveolar Progenitor Cell Metabolism in Response to Lung Injury. Stem Cell Reports. 2020; 14: 420–432. [Medline] [CrossRef]
22. Sanders JM, Monogue ML, Jodlowski TZ, Cutrell JB. Pharmacologic Treatments for Coronavirus Disease 2019 (COVID-19): A Review. JAMA. 2020; 323: 1824–1836. [Medline]
23. Goldman JD, Lye DCB, Hui DS, Marks KM, Bruno R, Montejano R, et al. GS-US-540-5773 Investigators. Remdesivir for 5 or 10 Days in Patients with Severe Covid-19. N Engl J Med. 2020; 383: 1827–1837. [Medline] [CrossRef]
24. Beigel JH, Tomashek KM, Dodd LE, Mehta AK, Zingman BS, Kalil AC, et al. ACTT-1 Study Group Members. Remdesivir for the Treatment of Covid-19 - Final Report. N Engl J Med. 2020; 383: 1813–1826. [Medline] [CrossRef]
25. Ibáñez S, Martínez O, Valenzuela F, Silva F, Valenzuela O. Hydroxychloroquine and chloroquine in COVID-19: should they be used as standard therapy? Clin Rheumatol. 2020; 39: 2461–2465. [Medline] [CrossRef]
26. Sun J, Chen Y, Fan X, Wang X, Han Q, Liu Z. Advances in the use of chloroquine and hydroxychloroquine for the treatment of COVID-19. Postgrad Med. 2020; 132: 604–613. [Medline] [CrossRef]
27. Yu B, Li C, Chen P, Zhou N, Wang L, Li J, et al. Low dose of hydroxychloroquine reduces fatality of critically ill patients with COVID-19. Sci China Life Sci. 2020; 63: 1515–1521. [Medline] [CrossRef]
28. Geleris J, Sun Y, Platt J, Zucker J, Baldwin M, Hripcsak G, et al. Observational study of hydroxychloroquine in hospitalized patients with Covid-19. N Engl J Med. 2020; 382: 2411–2418. [Medline] [CrossRef]
29. Mitja O, Corbacho-Monne M, Ubals M, Tebe C, Penafiel J, Tobias A, et al. Hydroxychloroquine for early treatment of adults with mild Coronavirus Disease 2019: a randomized-controlled trial. Clin Infect Dis. 2021; 73: e4073–e4081.
30. Abd-Elsalam S, Esmail ES, Khalaf M, Abdo EF, Medhat MA, Abd El Ghafar MS, et al. Hydroxychloroquine in the Treatment of COVID-19: A Multicenter Randomized Controlled Study. Am J Trop Med Hyg. 2020; 103: 1635–1639. [Medline] [CrossRef]
31. Rachidi S, Deng Z, Sullivan DY, Lipson EJ. Shorter survival and later stage at diagnosis among unmarried patients with cutaneous melanoma: A US national and tertiary care center study. J Am Acad Dermatol. 2020; 83: 1012–1020. [Medline] [CrossRef]
32. Stremmel C, Kellnar A, Massberg S, Kääb S. Hydroxychloroquine in COVID-19 Therapy: Protection Versus Proarrhythmia. J Cardiovasc Pharmacol Ther. 2020; 25: 497–502. [Medline] [CrossRef]
33. Elavarasi A, Prasad M, Seth T, Sahoo RK, Madan K, Nischal N, et al. Chloroquine and Hydroxychloroquine for the Treatment of COVID-19: a Systematic Review and Meta-analysis. J Gen Intern Med. 2020; 35: 3308–3314. [Medline] [CrossRef]
34. Infante M, Ricordi C, Alejandro R, Caprio M, Fabbri A. Hydroxychloroquine in the COVID-19 pandemic era: in pursuit of a rational use for prophylaxis of SARS-CoV-2 infection. Expert Rev Anti Infect Ther. 2021; 19: 5–16. [Medline] [CrossRef]
35. Rismanbaf A, Zarei S. Liver and Kidney Injuries in COVID-19 and Their Effects on Drug Therapy; a Letter to Editor. Arch Acad Emerg Med. 2020; 8: e17. [Medline]
36. Falcão MB, Pamplona de Góes Cavalcanti L, Filgueiras Filho NM, Antunes de Brito CA. Case Report: Hepatotoxicity Associated with the Use of Hydroxychloroquine in a Patient with COVID-19. Am J Trop Med Hyg. 2020; 102: 1214–1216. [Medline] [CrossRef]
37. Manivannan E, Karthikeyan C, Moorthy NSHN, Chaturvedi SC. The Rise and Fall of Chloroquine/Hydroxychloroquine as Compassionate Therapy of COVID-19. Front Pharmacol. 2021; 12: 584940. [Medline] [CrossRef]
38. Wang J, Li X, Wang A, Zhao F, Wu Q, Li L, et al. Organoid technology demonstrates effects of potential drugs for COVID-19 on the lung regeneration. Cell Prolif. 2020; 53: e12928. [Medline] [CrossRef]
39. Kamio K, Azuma A, Matsuda K, Usuki J, Inomata M, Morinaga A, et al. Resolution of bleomycin-induced murine pulmonary fibrosis via a splenic lymphocyte subpopulation. Respir Res. 2018; 19: 71. [Medline] [CrossRef]
40. Mikumo H, Yanagihara T, Hamada N, Harada E, Ogata-Suetsugu S, Ikeda-Harada C, et al. Neutrophil elastase inhibitor sivelestat ameliorates gefitinib-naphthalene-induced acute pneumonitis in mice. Biochem Biophys Res Commun. 2017; 486: 205–209. [Medline] [CrossRef]
41. Ip A, Ahn J, Zhou Y, Goy AH, Hansen E, Pecora AL, et al. Hydroxychloroquine in the treatment of outpatients with mildly symptomatic COVID-19: a multi-center observational study. BMC Infect Dis. 2021; 21: 72. [Medline] [CrossRef]
42. Meo SA, Klonoff DC, Akram J. Efficacy of chloroquine and hydroxychloroquine in the treatment of COVID-19. Eur Rev Med Pharmacol Sci. 2020; 24: 4539–4547. [Medline]
43. Sinha N, Balayla G. Hydroxychloroquine and COVID-19. Postgrad Med J. 2020; 96: 550–555. [Medline] [CrossRef]
44. Chen H, Matsumoto K, Brockway BL, Rackley CR, Liang J, Lee JH, et al. Airway epithelial progenitors are region specific and show differential responses to bleomycin-induced lung injury. Stem Cells. 2012; 30: 1948–1960. [Medline] [CrossRef]
45. Durcan L, Clarke WA, Magder LS, Petri M. Hydroxychloroquine Blood Levels in Systemic Lupus Erythematosus: Clarifying Dosing Controversies and Improving Adherence. J Rheumatol. 2015; 42: 2092–2097. [Medline] [CrossRef]

46. Masson JD, Blanchet B, Periou B, Authier FJ, Mograbi B, Gherardi RK, et al. Long Term Pharmacological Perturbation of Autophagy in Mice: Are HCQ Injections a Relevant Choice? Biomedicines. 2020; 8: 47. [Medline] [CrossRef]
47. Kong J, Wen S, Cao W, Yue P, Xu X, Zhang Y, et al. Lung organoids, useful tools for investigating epithelial repair after lung injury. Stem Cell Res Ther. 2021; 12: 95. [Medline] [CrossRef]
48. Schrezenmeier E, Dörner T. Mechanisms of action of hydroxychloroquine and chloroquine: implications for rheumatology. Nat Rev Rheumatol. 2020; 16: 155–166. [Medline] [CrossRef]
49. McCauley KB, Hawkins F, Serra M, Thomas DC, Jacob A, Kotton DN. Efficient Derivation of Functional Human Airway Epithelium from Pluripotent Stem Cells via Temporal Regulation of Wnt Signaling. Cell Stem Cell. 2017; 20: 844–857.e6. [Medline] [CrossRef]
50. Jacob A, Morley M, Hawkins F, McCauley KB, Jean JC, Heins H, et al. Differentiation of Human Pluripotent Stem Cells into Functional Lung Alveolar Epithelial Cells. Cell Stem Cell. 2017; 21: 472–488.e10. [Medline] [CrossRef]
51. Barkauskas CE, Chung MI, Fioret B, Gao X, Katsura H, Hogan BL. Lung organoids: current uses and future promise. Development. 2017; 144: 986–997. [Medline] [CrossRef]
52. Rock JR, Randell SH, Hogan BL. Airway basal stem cells: a perspective on their roles in epithelial homeostasis and remodeling. Dis Model Mech. 2010; 3: 545–556. [Medline] [CrossRef]